RESEARCH PAPER

Far-infrared spectroscopic study of CeO$_2$ nanocrystals

Z. V. Popović · M. Grujić-Brojčin · N. Paunović ·
M. M. Radonjić · V. D. Araújo · M. I. B. Bernardi ·
M. M. de Lima · A. Cantarero

Abstract We present the far-infrared reflectivity spectra of 5 nm-sized pure and copper-doped Ce$_{1-x}$Cu$_x$O$_{2-y}$ ($x = 0$; 0.01 and 0.10) nanocrystals measured at room temperature in the 50–650 cm^{-1} spectral range. Reflectivity spectra were analyzed using the factorized form of the dielectric function, which includes the phonon and the free carriers contribution. Four oscillators with TO energies of approximately 135, 280, 370, and 490 cm^{-1} were included in the fitting procedure. These oscillators represent local maxima of the CeO$_2$ phonon density of states, which is also calculated using the density functional theory. The lowest energy oscillator represents TA(L)/TA(X) phonon states, which become infrared-active E_u modes at the L and X points of the Brillouin zone (BZ). The second oscillator originates from TO(Γ) phonon states. The oscillator at ~400 cm^{-1} originates from Raman mode phonon states, which at the L point of BZ also becomes infrared-active E_u mode. The last oscillator describes phonons with dominantly LO(Γ) infrared mode character. The appearance of phonon density of states related oscillators, instead of single F_{2u} infrared-active mode in the far-infrared reflectivity spectra, is a consequence of the nanosized dimension of the CeO$_2$ particles. The best fit spectra are obtained using the generalized Bruggeman model for inhomogeneous media, which takes into account the nanocrystal volume fraction and the pore shape.

Keywords Nano ceria · Far-infrared spectroscopy · Phonon density of states · Bruggeman model · Nanoparticle characterization

Z. V. Popović (✉) · M. Grujić-Brojčin · N. Paunović
Center for Solid State Physics and New Materials,
Institute of Physics, University of Belgrade, Pregrevica
118, 11080 Belgrade, Serbia
e-mail: zoran.popovic@ipb.ac.rs

M. M. Radonjić
Scientific Computing Laboratory, Institute of Physics
Belgrade, University of Belgrade, Pregrevica 118,
11080 Belgrade, Serbia

V. D. Araújo · M. I. B. Bernardi
Instituto de Fisica, Universidade de São Paulo-USP,
São Carlos, SP 13560-970, Brazil

M. M. de Lima · A. Cantarero
Instituto de Ciencia de Los Materiales, Universidade de
Valencia, 46071 Valencia, Spain

Introduction

There are plenty of nanoscopic, microscopic, and other techniques that are used to study nanosized materials and structures (Popović et al. 2011). Among them, the most frequently used spectroscopic techniques are vibrational (phonon) spectroscopy techniques, such as Raman (R) and infrared (IR). The use of these techniques for nanostructure characterization is discussed in Popović et al. (2011), Grujić-Brojčin et al. (2005), and Cantarero (2013).

Ultrafine ceria powders represent an important material for solid oxide fuel cells or catalytic applications, which are attributed to CeO_2 remarkable oxygen-storage capability, i.e., the ability to undergo rapid redox cycles by releasing and storing oxygen (Popović et al. 2012).

In a nanocrystal, the phonons are confined in space, and all the phonons over the entire Brillouin zone (BZ) will contribute to the first-order vibrational spectra. The weight of the off-center phonons increases as the crystal size decreases, and the phonon dispersion causes a mode shape change and the frequency shift. The influence of all these effects on the CeO_2 Raman mode intensity, line shape, and energy were discussed in Popović et al. (2011) and Cantarero (2013).

Infrared spectroscopy is widely used in the 400–4,000 cm^{-1} spectral range to characterize unwished residuals during the synthesis of CeO_2 nanopowders (Orel 1999). To the best of our knowledge there are no study regarding infrared-active lattice vibrations in ceria nanocrystals. In this paper, we have measured room-temperature far-infrared reflectivity spectra of the pure and copper-doped $Ce_{1-x}Cu_xO_{2-y}$ ($x = 0$, 0.01 and 0.10) nanocrystals in the 50–650 cm^{-1} spectral range. In order to assign the obtained features we performed lattice dynamics calculation of CeO_2. Reflectivity spectra were analyzed using the factorized form of the dielectric function, which includes several oscillators and the free carriers contribution to the dielectric function. The oscillators represent the phonon density of states (PDOS)-related IR active modes. The best fit spectra are obtained using the generalized Bruggeman model for inhomogeneous media, which takes into account the volume fraction of nanopowder and the pore shape.

Experiment and numerical method

Ceria samples were prepared in one step by the polymeric precursor method (Araújo et al. 2013). The sizes of nanocrystals obtained by Raman scattering technique are about 5 nm. Specific surface area of the samples (BET-method) were estimated from the N_2-adsorption/desorption isotherms, at liquid nitrogen temperature, using a Micromeritics ASAP 2000 analyzer. The infrared reflectivity measurements were carried out at room temperature with a BOMEM DA-8

Fourier-transform IR spectrometer. A deuterated triglycine sulfate (DTGS) pyroelectric detector was used to cover the wave number region from 50 to 650 cm^{-1}. Spectra were collected with 2 cm^{-1} resolution, with 1,000 interferometer scans added for each spectrum.

In order to interpret the experimental data, we have performed density functional theory calculations implemented within the QUANTUM ESPRESSO package (Giannozzi et al. 2009). We have used the ultrasoft pseudopotentials with PBE exchange–correlation functional with $4f^1$, $5s^2$, $5p^6$, $5d^1$, $6s^2$ valence electrons of cerium and $2s^2$, $2p^4$ valence electrons of oxygen. The energy cutoffs for the wave functions and the electron densities were 60 and 900 Ry, determined to ensure stable convergence. We have sampled the BZ with a $32 \times 32 \times 32$ Monkhorst–Pack **k**-space mesh.

The phonon frequencies are calculated within density functional perturbation theory (Baroni et al. 2001), over the BZ sampled with $8 \times 8 \times 8$ Monkhorst–Pack **q**-point mesh. We have calculated the PDOS using that mesh, and the phonon dispersion curves are obtained from interpolation along the chosen path.

Results and discussion

Cerium dioxide crystallizes in the fluorite-type cubic crystal structure (Fig. 1), space group $Fm\bar{3}m$ (no. 225), in which Ce is located in (4a) (0,0,0), surrounded by eight oxygen atoms located at (8c) (1/4, 1/4, 1/4) Wyckoff positions. This structure has one infrared (F_{2u}) and one Raman (F_{2g}) active mode, each of them being triple degenerated. The normal modes of these vibrations are sketched in Fig. 1. The F_{2u} mode represents vibrations of both the Ce and O atoms in opposite directions, whereas F_{2g} mode originates from the stretching vibrations of only oxygen atoms around Ce. In the CeO_2 single crystals and polycrystalline samples, the infrared and Raman active modes appear at 283/596 cm^{-1} (ω_{TO}/ω_{LO}) (Marabelli and Wachter 1987; Santha et al. 2004) and 465 cm^{-1} (R) (Kourouklis et al. 1988; Weber et al. 1993; Nakajima et al. 1994), respectively. In our less than 5 nm CeO_{2-y} nanocrystals (Popović et al. 2012) the Raman mode is centered at about 456 cm^{-1}.
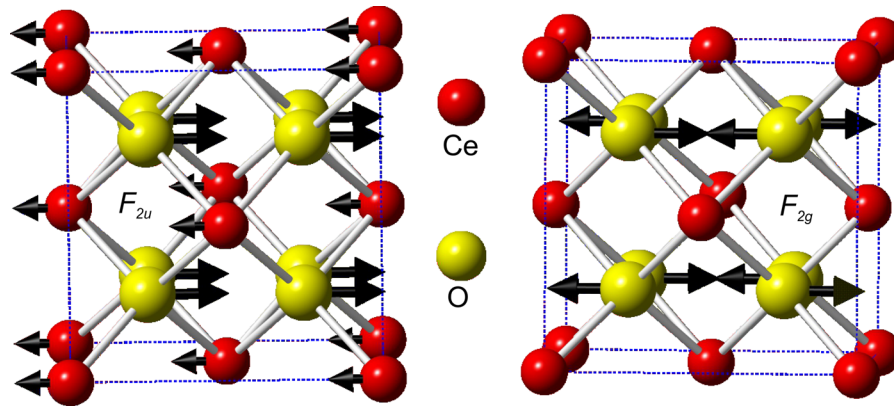
Fig. 1 The normal modes of the infrared (F_{2u}) and Raman (F_{2g}) active lattice vibrations of CeO$_2$ (Color online)

Because our nano CeO$_2$ samples are inhomogeneous (they consist of CeO$_2$ nanoparticles and air pores) we have applied the effective medium approximation (EMA) method to calculate infrared reflectivity of inhomogeneous media, taking into account the macroscopic volume fractions and local microstructural geometry (Grujić-Brojčin et al. 2005; Gonzalez et al. 1997; Spanier and Herman 2000; Bruggeman 1935). Two widely used effective medium theories are the Maxwell–Garnett theory (Maxwell–Garnett 1904) and the Bruggeman theory (Bruggeman 1935). In both theories the effective dielectric constant does not depend explicitly on the size of the grains or inclusions occurring inside the medium. Maxwell–Garnett approximation treats the effective medium as consisting of a matrix in which are embedded inclusions of a specific shape, where the fraction of the inclusions is very small (<0.15), so that the inclusions are spatially separated and can be treated as a perturbation (Spanier and Herman 2000; Saarinen et al. 2003; Gehr et al. 1997). The other widely used approximation is the Bruggeman's, which has no such limitations, and can be used for entire range of fraction values from 0 to 1. That was the reason why we used Bruggeman approach for analysis of infrared reflectivity spectra of inhomogeneous CeO$_2$ nanocrystals.

As nanophase CeO$_2$ is a porous material with a relatively large specific surface (see Table 1), the porosity of the nanopowder is included in modeling its dielectric function. The best agreement between calculated and experimental results is obtained by the generalized Bruggeman EMA (B-EMA), which introduces the effect of pore shape using the adjustable depolarization factor L for ellipsoidal voids ($L = 1/3$

for spherical cavities and $1/3 < L < 1$ for prolate spheroidal cavities).

Similar to the B-EMA, in the generalized Bruggeman model (Grujić-Brojčin et al. 2005, 2006; Spanier and Herman 2000), porous nanopowder with effective dielectric function $\varepsilon_{\mathrm{eff}}$ is assumed to be an inhomogeneous media composed of nanopowder ($\varepsilon_{\mathrm{nano}}$) and air ($\varepsilon_{\mathrm{air}} = 1$) with volume fractions f_{nano} and f_{air}, respectively. The basic Bruggeman model is modified to include the influence of porosity:

$$
\left(\frac{\varepsilon_{\mathrm{nano}} - \varepsilon_{\mathrm{eff}}}{\varepsilon_{\mathrm{eff}} + L(\varepsilon_{\mathrm{nano}} - \varepsilon_{\mathrm{eff}})}\right) f_{\mathrm{nano}}
$$
$$
+ \left(\frac{\varepsilon_{\mathrm{air}} - \varepsilon_{\mathrm{eff}}}{\varepsilon_{\mathrm{eff}} + L(\varepsilon_{\mathrm{air}} - \varepsilon_{\mathrm{eff}})}\right) f_{\mathrm{air}} = 0 \quad (1)
$$

Generally, a decrease of nanopowder volume fraction results in a decrease of reflectivity and broadening of the IR features, due to the greater air fraction in the powder. Also, the decrease of depolarization factor L, from prolate spheroidal voids ($L = 1$) to spherical pores ($L = 1/3$), leads to the increase in the reflectivity, with characteristic IR features becoming more pronounced (Grujić-Brojčin et al. 2005).

Since the analysis of the far IR reflectivity spectrum of ceria nanopowders has revealed a presence of a plasmon mode, it was necessary to include both contributions of the phonon and the plasmon (free carrier contribution) to the dielectric function. Therefore, the factorized form of dielectric function has been decomposed into a sum of two independent terms (Gonzalez et al. 1997; Grujić-Brojčin et al. 2006; Gervais 1983):

Table 1 The characteristic TO and LO phonon frequencies (ω) and damping factors (γ) (all given in cm^{-1}) of Ce$_{1-x}$Cu$_x$O$_{2-y}$ nano- and poly-crystals, used in the fitting procedure together with the corresponding plasmon parameters for pure, 1, and 10 % Cu-doped CeO$_2$ samples

Parameters	0 % Cu	1 % Cu	10 % Cu	10 nm nano	Polycrystal
ω_{TO} (γ_{TO})	135 (190)	137 (220)	137 (300)	130 (132)	135 (130)
ω_{LO} (γ_{LO})	155 (95)	147 (180)	147 (180)	160 (188)	161 (187)
ω_{TO} (γ_{TO})	282 (37)	280 (28)	280 (25)	273 (57)	272 (25)
ω_{LO} (γ_{LO})	375 (180)	380 (165)	385 (180)	280 (108)	416 (137)
ω_{TO} (γ_{TO})	370 (100)	360 (95)	370 (140)	448 (159)	–
ω_{LO} (γ_{LO})	407 (100)	407 (150)	407 (120)	468 (105)	–
ω_{TO} (γ_{TO})	490 (180)	480 (140)	485 (180)	493 (113)	428 (157)
ω_{LO} (γ_{LO})	580 (10)	580 (60)	585 (40)	585 (385)	587 (47)
ω_{TO} (γ_{TO})	–	–	–	333 (67)	–
ω_{LO} (γ_{LO})	–	–	–	350 (88)	–
ω_p (γ_p)	390 (400)	385 (580)	320 (550)	100 (50)	–
f_{nano}	0.80	0.83	0.86		
Pore shape L	0.74	0.70	0.70		
Specific surface area S$_{BET}$ (m^2/g)	40	40	44		
Average pore diameter (nm)	10.8	12.4	9.1		

The fitting parameters from Bruggeman model (powder volume fraction f_{nano} and the pore shape L) together with the specific surface area and pore diameter values are listed for each nanopowder sample

$$\varepsilon(\omega) = \varepsilon_\infty \left[\prod_{j=1}^{n} \frac{\omega_{LO,j}^2 - \omega^2 + i\omega\gamma_{LO,j}}{\omega_{TO,j}^2 - \omega^2 + i\omega\gamma_{TO,j}} - \frac{\omega_p^2}{\omega(\omega - i\gamma_p)} \right] \tag{2}$$

where $\omega_{LO,j}$ and $\omega_{TO,j}$ are longitudinal and transverse frequencies of the jth oscillator, $\gamma_{LO,j}$ and $\gamma_{TO,j}$ are their corresponding dampings, ω_p (γ_p) is the plasma frequency (damping), and ε_∞ is the high-frequency dielectric constant.

Figure 2a shows the PDOS of CeO$_2$. This PDOS is in complete agreement with previously published ones (Marabelli and Wachter 1987; Nakajima et al. 1994; Gürel and Eryiğit 2006; Buckeridge et al. 2013).

The CeO$_2$ IR reflectivity spectra of polycrystalline sample (Santha et al. 2004) and 10-nm particle size undoped CeO$_2$ nanocrystal are given in Fig. 2b, c, respectively. These spectra are fitted using dielectric function model, Eq. (2), with parameters given in Table 1. In the case of the polycrystalline sample three oscillators are used to obtain a rather good agreement with experimental data. The lowest energy oscillator with TO energy of 135 cm^{-1} represents phonon states from the X and L point of BZ. Other two oscillators represent F_{2u} mode. Appearance of two instead of one IR active mode in this spectral range is related to the anharmonicity (Santha et al. 2004). In the case of the
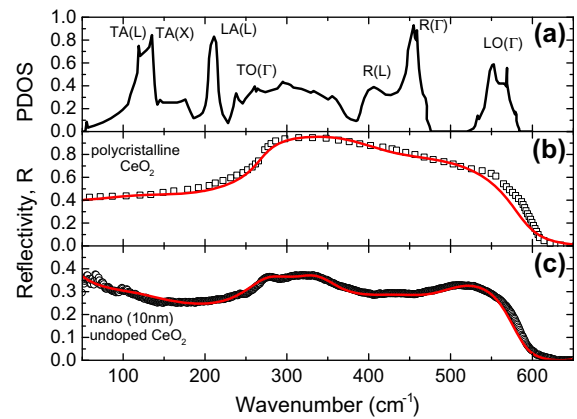

Fig. 2 a The phonon density of states of CeO$_2$. **b** The IR reflectivity spectra of polycrystalline CeO$_2$ sample (Santha et al. 2004); **c** nanocrystalline undoped CeO$_2$ sample (particle size ∼10 nm). *Solid lines* represent the calculated reflectivity spectra obtained by the fitting procedure based on Eq. (2), with the parameters given in Table 1 (Color online)

nanosized sample (Fig. 2c) five oscillators are included in the fitting procedure, as well as, plasma term (see Table 1). Origin of these oscillators will be discussed later.

The influence of nanopowder volume fraction and the pore shape on the IR reflectivity spectra is analyzed in Fig. 3a–c, which show the IR reflectivity spectra

calculated with the generalized B-EMA, with the variation of powder volume fraction f_{nano} and fixed value of depolarization factor (pore shape factor) $L = 0.33$, 0.75, and 0.90, respectively. The spectra are calculated with the set of parameters corresponding to the pure CeO_2 sample, listed in the Table 1 (0 % Cu), whereas f_{nano} is varied from 0.5 (50 % of CeO_2 powder in porous sample) to 1 (nonporous powder). The pore shape factor $L = 0.33$ defines ideally spherical pores and for given TO/LO parameters, the best volume fraction fit corresponds to values of f_{nano} between 50 and 60 % of powder content in the sample (Fig. 3a).

The pore shape factor $L = 0.75$ defines pores with elongated structure, as indicated in Fig. 3b. For given TO/LO parameters (Table 1) the best volume fraction fit corresponds to values of f_{nano} around 80 % of powder content in the sample. In Fig. 3c the variation of powder volume fraction f_{nano} with depolarization factor $L = 0.90$ is shown. The pore shape factor $L = 0.90$ corresponds to extremely elongated pores.

For given TO/LO parameters (Table 1) the best volume fraction fit corresponds to values of f_{nano} between 80 and 90 % of powder content in the sample.

The pore shape variation is analyzed in Fig. 3d–f. In Fig. 3d the calculated spectrum for powder volume fraction $f_{nano} = 1$, i.e., nonporous powder is shown together with experimental IR reflectivity of the pure CeO_2 sample. The spectrum is calculated with the set of parameters corresponding to the pure CeO_2 sample, listed in Table 1 (0 % Cu), whereas the pore shape factor (L) variation has no influence in this calculation. Figure 3e, f show the IR reflectivity spectra calculated with the generalized Bruggeman EMA with powder volume fraction of 80 % and 50 %. The pore shape factor varied from $L = 0.3$–0.9. It may be noticed that in both cases, the intensity of the reflectivity is getting lower with the increase in pore shape factor. For given TO/LO parameters (Table 1) the best pore shape fit is obtained for values of L from 0.7 to 0.8 (Fig. 3e), corresponding to the area of elongated pores. These
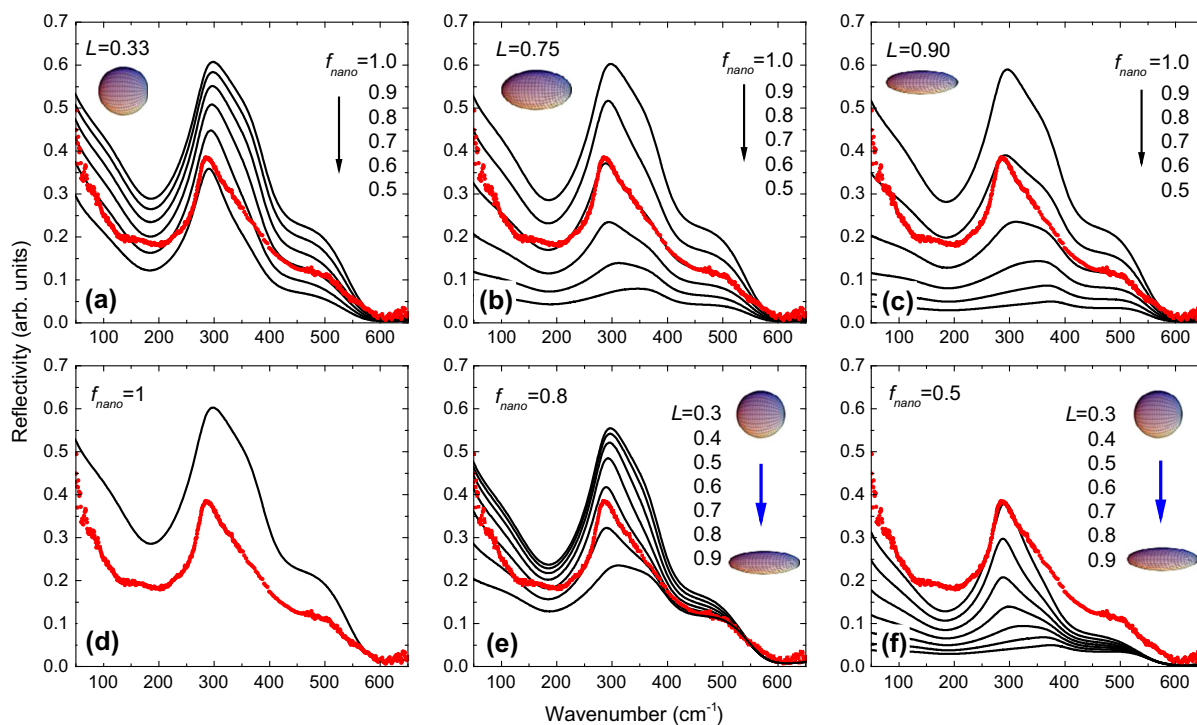

Fig. 3 The IR reflectivity spectra calculated with the generalized B-EMA. **a** The volume fraction of nanopowder is in the range from 0.5 to 1.0 and the pore shape factor $L = 0.33$ (spherical shape of pores); **b** pore shape factor $L = 0.75$ (elongated pore structure); **c** pore shape factor $L = 0.90$ (extremely elongated pore structure); **d** the IR reflectivity spectra calculated with the generalized B-EMA with the volume fraction of the nanopowder $f_{nano} = 1$ (nonporous powder); **e** fixed volume fraction of nanopowder ($f_{nano} = 0.8$) with pore shape factor varying from 0.3 to 0.9; **f** fixed volume fraction of nanopowder ($f_{nano} = 0.5$) with pore shape factor varying from 0.3 to 0.9. Experimental IR reflectivity spectrum (*red curve*) of pure CeO_2 sample (0 % Cu) is given for comparison (Color online)

results correspond to those shown in Fig. 3b. Finally, in Fig. 3f the best pore shape fit is obtained for values of L around 0.3, corresponding to ideally spherical pores.

By analyzing the results shown in Fig. 3, we came to the following conclusions:

(i)   Bruggeman EMA model can be used to fit the experimental reflectivity spectra of inhomogeneous nanomaterials, in our case CeO_2 nanocrystals.

(ii) The B-EMA model parameters that best describe the experimental CeO_2 reflectivity spectra are close to $f_{nano} = 0.8$ and $L = 0.75$. (see Fig. 3b). Refinement of these parameters for samples under investigation gives values shown in Table 1.

(iii) The very good agreement between the calculated and the experimental spectra illustrated in Fig. 4 suggests that the use of more specific model, which may include the pore shape distribution, instead of the B-EMA general and simple model, is not necessary.

In Fig. 4 experimental IR reflectivity spectra of 5 nm-sized pure, 1, and 10 % Cu-doped CeO_2 samples are shown, together with the corresponding spectra calculated with the generalized B-EMA. Fitting parameters for these spectra are listed in Table 1. As can be seen from Table 1, four oscillators with TO energies of approximately 135, 280, 370, and 490 cm^{-1} were included in the fitting procedure, Eq. (2), for 5 nm-sized CeO_2 samples. These
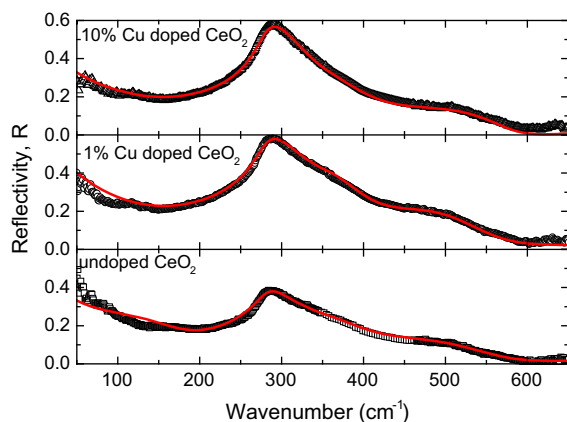

Fig. 4 Experimental IR reflectivity spectra of pure, 1, and 10 % Cu-doped CeO_2 samples, with the corresponding spectra obtained by the fitting procedure based on Eq. (2) and the generalized B-EMA, Eq. (1). Parameters are given in Table 1

oscillators represent local maxima of the PDOS. The lowest energy oscillator represents TA(L)/TA(X) phonon states, which become IR-active E_u modes (Buckeridge et al. 2013) at the L and X points of BZ. The second oscillator originates from TO(Γ) phonon states. The oscillator at ~ 400 cm^{-1} originates from Raman mode phonon states which at the L point of BZ also becomes IR-active E_u mode (Buckeridge et al. 2013). The last oscillator describes phonons with dominantly LO(Γ) IR mode character. The appearance of PDOS-related oscillators, instead of single F_{2u} IR-active mode in the far-infrared reflectivity spectra, is a consequence of the nanosized dimension of the particles, as mentioned earlier. Besides that, the oscillator energies appear at lower energies than the maxima of PDOS. This is also related to the particle size. In fact, in nanoceria the unit cell dimensions abruptly increase by particle size reduction (Tsunekawa et al. 2000; Wu et al. 2004). Consequently, the PDOS softens with the particle size lowering due to an increase in the internal strain, as it was discussed in Buckeridge et al. (2013).

A small variation in the frequencies of TO (LO) modes of the pure and doped samples is noticed, whereas the damping parameters are clearly affected by the variation between pure and doped samples. Plasmon modes are registered in all samples, with significant plasma frequency decrease and damping parameter increase with Cu doping. The values of parameters used in the generalized Bruggeman EMA are varied with doping: similar porosity has been estimated in all studied samples. Namely, the volume fraction parameter is estimated from $f_{nano} = 0.80$ in pure CeO_2 (which means 80 % of CeO_2 fraction in a porous sample) to 0.86 in 10 % Cu-doped CeO_2 sample. The depolarization factor L, defining pore shape is estimated as 0.74 in pure CeO_2 sample and slightly lower (0.70) in doped samples, therefore describing pores filled with the air as very elongated. Comparing these with textural measurement results, we find that in the 10 % Cu-doped sample, the reduction of L and an increase in volume fraction is correlated with a decrease of pore diameter and an increase in specific surface area (see Table 1).

Conclusion

We have measured the unpolarized far-infrared reflectivity spectra of the CeO_2 nanocrystals at room

temperature. Reflectivity spectra were analyzed using the factorized form of the dielectric function, which includes the phonon and plasmon contribution to the dielectric function. The best fit spectra are obtained using the generalized Bruggeman model for inhomogeneous media, which takes into account the volume fraction of CeO_2 nanocrystal and the air pore shape.

References

Araújo VD, de Lima MM Jr, Cantarero M, Bernardi MIB, Bellido JDA, Assaf EM, Balzer R, Probst LFD, Fajardo HV (2013) Catalytic oxidation of n-hexane promoted by $Ce_{1-x}Cu_xO_2$ catalysts prepared by one-step polymeric precursor method. Mater Chem Phys 142:677–681

Baroni S, de Gironcoli S, Dal Corso A, Giannozzi P (2001) Phonons and related crystal properties from density-functional perturbation theory. Rev Mod Phys 73:515–562

Bruggeman DAG (1935) Berechnung verschiedener physikalischer Konstanten von heterogenen Substanzen. I. Dielektrizitätskonstanten und Leitfähigkeiten der Mischkörper aus isotropen Substanzen. Ann Phys 24:636–664

Buckeridge J, Scanlon DO, Walsh A, Catlow CRA, Sokol AA (2013) Dynamical response and instability in ceria under lattice expansion. Phys Rev B 87(21):214304

Cantarero A (2013) Review on Raman scattering in semiconductor nanowires: I. Theory. J Nanophotonics 7(1):071598

Gehr RJ, Fischer GL, Boyd RW (1997) Nonlinear-optical response of porous-glass-based composite materials. J Opt Soc Am B 14(9):2310–2314

Gervais F (1983) High-temperature infrared reflectivity spectroscopy by scanning interferometry. In: Button KJ (ed) Infrared and millimeter waves. Academic Press, New York, pp 279–339

Giannozzi P, Baroni S, Bonini N, Calandra M, Car R, Cavazzoni C, Ceresoli D, Chiarotti GL, Cococcioni M, Dabo I, Corso AD, de Gironcoli S, Fabris S, Fratesi G, Gebauer R, Gerstmann U, Gougoussis C, Kokalj A, Lazzeri M, Martin-Samos L, Marzari N, Mauri F, Mazzarello R, Paolini S, Pasquarello A, Paulatto L, Sbraccia C, Scandolo S, Sclauzero G, Seitsonen AP, Smogunov A, Umari P, Wentzcovitch RM (2009) QUANTUM ESPRESSO: a modular and open-source software project for quantum simulations of materials. J Phys 21(39):395502

Gonzalez RJ, Zallen R, Berger H (1997) Infrared reflectivity and lattice fundamentals in anatase TiO_2. Phys Rev B 55(11):7014–7017

Grujić-Brojčin M, Šćepanović MJ, Dohčević-Mitrović ZD, Hinić I, Matović B, Stanišić G, Popović ZV (2005) Infrared study of laser synthesized anatase TiO_2 nanopowders. J Phys D 38(9):1415–1420

Grujić-Brojčin M, Šćepanović MJ, Dohčević-Mitrović ZD, Popović ZV (2006) Infrared study of nonstoichiometric anatase TiO_2 nanopowders. Sci Sinter 38:183

Gürel T, Eryiğit R (2006) Ab initio pressure-dependent vibrational and dielectric properties of CeO_2. Phys Rev B 74(1):014302

Kourouklis GA, Jayaraman A, Espinosa GP (1988) High-pressure Raman study of CeO_2 to 35 GPa and pressure-induced phase transformation from the fluorite structure. Phys Rev B 37(8):4250–4253

Marabelli F, Wachter P (1987) Covalent insulator 2: optical reflectivity measurements. Phys Rev B 36(2):1234–1238

Maxwell-Garnett JC (1904) Colours in metal glasses and in metallic films. Philos Trans R Soc Lond, Ser.4 203:385–420

Nakajima A, Yoshihara A, Ishigame M (1994) Defect-induced Raman spectra in doped CeO_2. Phys Rev B 50(18):13297–13307

Orel Z (1999) Characterization of cerium dioxide dip-coated films by spectroscopic technique. Internet J Vib Spec Vol 3, Edition 4, Section 6 (www.ijvs.com). Accessed 20 June 2013

Popović ZV, Dohčević-Mitrović Z, Šćepanović M, Grujić-Brojčin M, Aškrabić S (2011) Raman scattering on nanomaterials and nanostructures. Ann Phys 523(1–2):62–74

Popović ZV, Dohčević-Mitrović ZD, Paunović N, Radović M (2012) Evidence of charge delocalization in $Ce_{1-x-}Fe_{x}^{2+(3+)}O_{2-y}$ nanocrystals ($x = 0$, 0.06, 0.12). Phys Rev B 85:014302

Saarinen JJ, Vartiainen EM, Peiponen KE (2003) On tailoring of nonlinear spectral properties of nanocomposites having Maxwell Garnett or Bruggeman structure. Opt Rev 10(2):111–115

Santha NI, Sebastian MT, Mohanan P, Alford NM, Sarma K, Pullar RC, Kamba S, Pashkin A, Samukhina P, Petzelt J (2004) Effect of doping on the dielectric properties of cerium oxide in the microwave and far-infrared frequency range. J Am Ceram Soc 87(7):1233–1237

Spanier JE, Herman IP (2000) Use of hybrid phenomenological and statistical effective-medium theories of dielectric functions to model the infrared reflectance of porous SiC films. Phys Rev B 61(15):10437–10450

Tsunekawa S, Ishikawa K, Li ZQ, Kawazoe Y, Kasuya A (2000) Origin of anomalous lattice expansion in oxide nanoparticles. Phys Rev Lett 85(16):3440–3443

Weber WH, Hass KC, McBride JR (1993) Raman study of CeO_2: second-order scattering, lattice dynamics, and particle-size effects. Phys Rev B 48(1):178–185

Wu L, Wiesmann HJ, Moodenbaugh AR, Klie RF, Zhu Y, Welch DO, Suenaga M (2004) Oxidation state and lattice expansion of CeO_{2-x} nanoparticles as a function of particle size. Phys Rev B 69(12):125415